

# Excellence in Chemistry Research

## Announcing our new flagship journal

- Gold Open Access
- Publishing charges waived
- Preprints welcome
- Edited by active scientists



## Meet the Editors of *ChemistryEurope*



**Luisa De Cola**

Università degli Studi  
di Milano Statale, Italy



**Ive Hermans**

University of  
Wisconsin-Madison, USA



**Ken Tanaka**

Tokyo Institute of  
Technology, Japan

# Deinterpenetration of IRMOF-9

Audrey B. Crom,<sup>[b]</sup> Joseph L. Strozier,<sup>[a]</sup> Caleb J. Tatebe,<sup>[a]</sup> Cassidy A. Carey,<sup>[c]</sup>  
Jeremy I. Feldblyum,<sup>\*[b]</sup> and Douglas T. Genna<sup>\*[a]</sup>

One of the iconic characteristics of metal-organic frameworks (MOFs) is the possession of guest-accessible pores. Increasing pore size has a direct and often beneficial impact on a MOF's adsorption and separation properties. However, as pore size increases, the resulting void spaces are often filled by interpenetrated frameworks, where one or more networks crystallize within the pore system of another identical network, reducing the MOF's free volume and pore size. Furthermore, due to the thermodynamic favorability of interpenetration during solvothermal synthesis, techniques to synthetically differentiate inter-

penetrated from non-interpenetrated MOFs are paramount. This study reports the synthesis of deinterpenetrated IRMOF-9 via halide mediated deinterpenetrative conversion of Zn<sub>4</sub>O-derived IRMOF-9. IRMOF-9, when treated with ethylammonium bromide, is quasi-selectively etched, revealing the non-interpenetrated analogue, IRMOF-10 (deinterpenetrated IRMOF-9), which can be isolated prior to complete dissolution by the bromide solution. Dye adsorption, surface area and pore size distribution analysis, and powder X-ray diffraction are consistent with successful deinterpenetration.

## Introduction

Metal-organic frameworks (MOFs)<sup>[1]</sup> have become gradually more popular due to their promising potential in applications such as molecular storage/separations,<sup>[2]</sup> catalysis,<sup>[3]</sup> drug delivery,<sup>[4]</sup> etc.<sup>[5]</sup> As demands for greater storage capacity increased, the race to systematically synthesize larger and larger pore volumes began in earnest with the IRMOF (isorecticular MOF) series.<sup>[6]</sup> However, as the pore sizes and void volumes increased, it became possible for additional frameworks to grow within these voids. The resulting materials, known as interpenetrated MOFs<sup>[7]</sup> maximized packing efficiency while simultaneously decreasing guest storage capacities and available pore volume.<sup>[8]</sup>

In most cases, the interpenetrated isomer of a MOF is thermodynamically favored.<sup>[8a]</sup> In order to control the outcome of a given MOF synthesis and directly yield the non-interpenetrated framework,<sup>[9]</sup> solvothermal synthesis under signifi-

cant dilution (when compared to their interpenetrated counterparts) is generally necessary.<sup>[10]</sup> However, this approach leads to large amounts of waste, low yields, and often phase-impure material.

Previously, our group reported the halide-mediated penetration of the [In(CO<sub>2</sub>R)<sub>4</sub>]<sup>−</sup>-derived 3-dimensional MOF ATF-1 to the non-interpenetrated 2-dimensional isomer YCM-21.<sup>[11]</sup> This transformation is proposed to proceed through the temporary formation of an [In(CO<sub>2</sub>R)<sub>3</sub>X]<sup>−</sup> (X=halide) inorganic-node formed by the reaction of the [In(CO<sub>2</sub>R)<sub>4</sub>]<sup>−</sup> with exogenous halide. This halogenated intermediate allows for the interpenetrated frameworks to “unhook” from each other, prior to reformation of the [In(CO<sub>2</sub>R)<sub>4</sub>]<sup>−</sup> center. Once this unhooking mechanism occurs across the totality of the MOF, two independent frameworks are formed.

We hypothesized that a similar strategy could be employed with MOFs containing the Zn<sub>4</sub>O(CO<sub>2</sub>R)<sub>6</sub> cluster commonly found in the IRMOF series, thus allowing for the synthesis of deinterpenetrated IRMOFs from their interpenetrated counterparts. Herein we report the successful deinterpenetration of IRMOF-9.

## Results/Discussion

The IRMOF-9/IRMOF-10 isomeric pair derived from the Zn<sub>4</sub>O-cluster and 4,4'-biphenyldicarboxylic acid (H<sub>2</sub>BPDC) has been studied extensively<sup>[10b,12]</sup> since its original report by Yaghi.<sup>[6]</sup> Phase pure synthesis of IRMOF-10 has been difficult to achieve and characterize.

When we applied our optimized conditions for deinterpenetration, which were previously developed for the conversion of ATF-1 to YCM-21<sup>[11]</sup> (0.16 M solution of Et<sub>4</sub>NBr in DMF:CH<sub>2</sub>Cl<sub>2</sub> (1:1 v:v) at 120 °C), for the deinterpenetration of IRMOF-9 (synthesized using the protocol from Rowsell and Yaghi<sup>[12a]</sup>), the MOF visibly displayed signs of dissolution after 24 h. However, when IRMOF-9 was subjected to the same reaction solution at

[a] J. L. Strozier, C. J. Tatebe, Prof. D. T. Genna  
Department of Chemistry WBSH5053  
Youngstown State University  
Youngstown, OH 44555 (USA)  
E-mail: dtgenna@ysu.edu

[b] A. B. Crom, Prof. J. I. Feldblyum  
Department of Chemistry  
University at Albany, State University of New York  
Albany, NY 12222 (USA)  
E-mail: jfeldblyum@albany.edu

[c] C. A. Carey  
Department of Chemistry  
University of Michigan  
Ann Arbor, MI 48105 (USA)

Supporting information for this article is available on the WWW under <https://doi.org/10.1002/chem.202302856>

© 2023 The Authors. Chemistry - A European Journal published by Wiley-VCH GmbH. This is an open access article under the terms of the Creative Commons Attribution Non-Commercial NoDerivs License, which permits use and distribution in any medium, provided the original work is properly cited, the use is non-commercial and no modifications or adaptations are made.

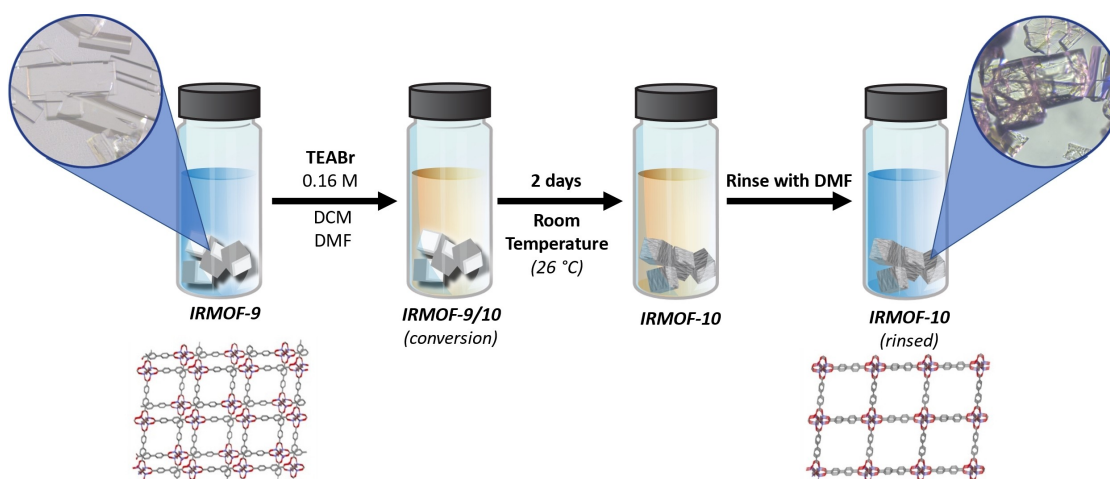


Figure 1. Synthesis of IRMOF-10 by deinterpenetrative conversion of IRMOF-9.

room temperature instead of 120 °C (Figure 1), no dissolution was observed. Analysis with both PXRD (Figure S1) and optical microscopy (Figure S2) indicated that the crystalline structure was intact albeit diminished after 2 days. However, due to the stress induced on the framework during conversion, the crystal quality of the product was not sufficient to obtain a crystallographic model from single-crystal X-ray diffraction. Furthermore, attempts to obtain IRMOF-10 directly with a one-pot solvothermal synthesis using  $\text{Zn}(\text{NO}_3)_2$ ,  $\text{H}_2\text{BPDC}$ , and  $\text{Et}_4\text{NBr}$  yielded neither IRMOF-10 nor IRMOF-9, regardless of the conditions tested.

UV-vis analysis of the deinterpenetrative conversion reaction solution indicated the presence of BPDC (Figure S3).  $^1\text{H}$  NMR of the mother liquor of the reaction revealed the presence of BPDC as well (Figure S4). Additionally, after 5 h, the MOF was filtered from the deinterpenetration solution and that solution was placed in a 100 °C oven for 24 h (the conditions necessary to grow IRMOF-9/10). Analysis after heating revealed the presence of inorganic Zn, which precipitated from solution as confirmed by PXRD analysis (Figure S5).

The presence of both BPDC and  $\text{Zn}^{2+}$  in the deinterpenetration reaction solution supports the contention that IRMOF-9 is being altered via partial dissolution. This can involve either (1) preferential dissolution of just one of the framework nets, leading to deinterpenetrated IRMOF-9 (IRMOF-10) or (2) indiscriminate dissolution across both frameworks yielding a material that resembles IRMOF-9 with pockets of hierarchical mesoporosity. These dissolution pathways were distinguished from each other using  $\text{N}_2$  gas sorption analysis and dye uptake exclusion experiments.

As no single crystal structure of unfunctionalized IRMOF-10 has been reported in the literature, the synthesis of IRMOF-10 is often confirmed by comparison with the calculated powder X-ray diffraction (PXRD) pattern of IRMOF-12.<sup>[13]</sup> However, both IRMOF-9 and IRMOF-12 share many common peaks in their respective PXRD patterns (notably at 5°, 7.3°, 10.3°, and 11.6° 2 $\theta$ ; Figure S6). Additionally, the calculated PXRD patterns for IRMOF-9 and IRMOF-10 are nearly identical (whether by

simulating IRMOF-10 as cubic by modifying IRMOF-12 or as triclinic by manually de-interpenetrating IRMOF-9), rendering their differentiation challenging (Figure S6).

Since it is challenging to rely solely on PXRD analysis to differentiate between IRMOF-9 and IRMOF-10, both pore size distribution (PSD) calculations and surface area measurements were used to distinguish the two MOFs. PSD analysis on both IRMOF-9 and its deinterpenetrated counterpart were initially carried out using density functional theory (DFT) to model experimental isotherms. PSD analysis of IRMOF-9 (Figures 2c and S7) revealed the presence of two pores, with the overwhelming majority having a diameter of 9.9 Å and a minority of

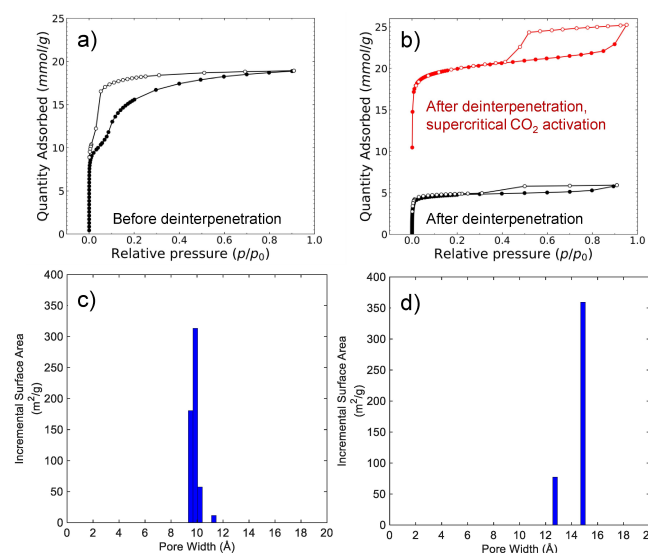


Figure 2. a)  $\text{N}_2$  sorption isotherm of IRMOF-9 activated at room temperature and reduced pressure (~200 mTorr) for 48 hours. b)  $\text{N}_2$  sorption isotherm of deinterpenetrated IRMOF-9 activated at room temperature and reduced pressure (~200 mTorr) for 24 hours (black trace) or with flowing supercritical  $\text{CO}_2$  (red trace; ●, adsorption; ○, desorption). c) Pore diameter distribution for IRMOF-9 based on a DFT fit. The majority pore diameter is 9.9 Å. d) Pore diameter distribution for deinterpenetrated IRMOF-9 based on DFT fit. The majority pore-diameter is 14.9 Å.



pores of 11.3 Å. Deinterpenetrated IRMOF-9, which was synthesized via de-interpenetrative conversion, exhibited two pore sizes with the majority having a diameter of 14.9 Å and a small minority of 12.7 Å (Figures 2d and S8). The observed diameters of the major pores of both IRMOF-9 and its deinterpenetrated counterpart (9.9 Å and 14.9 Å, respectively) are consistent with the expected values for the MOFs as previously determined from theoretical structures of both IRMOF-9 and IRMOF-10.<sup>[6]</sup> These findings are consistent with the formation of an IRMOF-10-like material, as opposed to an IRMOF-9 framework etched with meso/macropores (a “Swiss cheese” model). IRMOF-9 with hierarchical mesoporosity would exhibit a broad pore size distribution including pores larger than 14.9 Å while still possessing the smaller 9.9 Å and 11.3 Å pores of IRMOF-9 (attributable to the remaining portion of the still-interpenetrated framework).

Analysis of the N<sub>2</sub> isotherms of IRMOF-9 and its deinterpenetrated counterpart (both activated from dichloromethane) revealed BET surface areas of 1168 m<sup>2</sup>/g and 412 m<sup>2</sup>/g, respectively (Figures 2a and 2b, S9 and S10). It is worth noting that the N<sub>2</sub> isotherm of IRMOF-9 displays a two-step adsorption followed by significant hysteresis in the desorption curve in the 0–0.4 P/P<sub>0</sub> pressure range. This unusual behavior is indicative of structural changes leading to pore expansion (i.e., gating behavior), as previously reported during N<sub>2</sub> and CO<sub>2</sub> adsorption by Doonan and coworkers.<sup>[13]</sup> Canossa and Bacchi have reported the solvent-induced breathing/flexibility behavior of IRMOF-9 (as solved by single crystal X-ray diffraction using synchrotron irradiation) in the presence of DMF, 2-propanol, and CH<sub>2</sub>Cl<sub>2</sub>.<sup>[14]</sup> Furthermore, the shape of the isotherm matches that previously observed for flexible interpenetrated frameworks;<sup>[15]</sup> in contrast, the isotherm for deinterpenetrated IRMOF-9 does not exhibit this low-pressure hysteresis, nor does it possess any discernable steps. As unselective etching would not change the micropore size or dynamic behavior of the remaining material, the increased micropore size and lack of low-pressure hysteresis of the post-etched material point to conversion to IRMOF-10, rather than a simple introduction of meso- and/or macropore defects into IRMOF-9.

Our deinterpenetrated IRMOF-9 does exhibit a degree of pore collapse during activation prior to the collection of N<sub>2</sub> isotherm data (see Figure S11 for PXRD patterns before and after activation). Large pore zinc MOFs, for example, Zn-BPDC MOFs, have been shown to undergo pore collapse under even low mechanical stress, such as that which the MOF would be exposed to under conventional reduced pressure activation conditions.<sup>[16]</sup> Rapid desolvation has been shown to result in structural collapse of large-pore Zn<sub>4</sub>O MOFs due to a slip of the {100} layers in the <001> direction.<sup>[17]</sup>

To reduce the extent of pore collapse, the deinterpenetrated sample was activated with flowing supercritical CO<sub>2</sub>.<sup>[18]</sup> Analysis by N<sub>2</sub> gas sorption revealed a BET surface area of 1778 m<sup>2</sup>/g – substantially higher than that achieved both with the parent IRMOF-9 and with the deinterpenetrated sample activated under reduced pressure. X-ray diffraction after activation shows broader reflections suggestive of some loss of crystalline order, but well-matched to those expected for

IRMOF-10 (Figure S12) and better defined than those observed after activation under reduced pressure (Figure S11). These data are consistent with successful deinterpenetration of IRMOF-9.

Given some loss in crystallinity during activation, the structural integrity of the pores of deinterpenetrated IRMOF-9 prior to activation was established by size exclusion dye uptake experiments. As previously reported by Yaghi,<sup>[6]</sup> IRMOF-9 has an accessible pore aperture of 10.6 Å while IRMOF-10 has an accessible pore aperture of 15.4 Å. However, we conducted our own assessment of the pore size apertures of both IRMOF-9 and IRMOF-10 using PoreBlazer.<sup>[19]</sup> These simulations revealed that the apertures are smaller than originally reported, with IRMOF-9 having a pore aperture of only 8.1 Å and IRMOF-10 having an aperture of 11.7 Å. Treatment of IRMOF-10 with a solution of Reichardt's dye (kinetic diameter ~11 Å) should lead to dyed crystals, while treatment of IRMOF-9 with the same dye solution should yield colorless crystals. Thus, IRMOF-9 was deinterpenetrated in the presence of Reichardt's dye, and the conversion was monitored *in situ* and confirmed via dye uptake. First, IRMOF-9 was immersed in a solution of 0.16 M Et<sub>4</sub>NBr in a 1:1 DMF:DCM solution in the presence of 10 mM Reichardt's dye. The reaction was then monitored at regular time intervals by washing the crystals with fresh DCM and analyzing extent of dye uptake via optical microscopy (Figure 3). This *in situ* dye uptake study revealed that deinterpenetration occurs after 2 days at room temperature. After this time, the MOF crystals exhibited a blue color throughout, indicating the successful uptake of Reichardt's dye and deinterpenetration of IRMOF-9.

Uptake into the MOF's interior can be distinguished from dye adsorption to the exterior MOF surface by examining the cross-sections of these MOFs via optical microscopy. Cross-section analysis of the *in situ* deinterpenetrated IRMOF-9 indicated that the dye was persistent throughout the crystal. Importantly, when as-synthesized IRMOF-9 was subjected to 10 mM Reichardt's dye in DMF, cross-sectional analysis confirmed no dye was incorporated within the crystal (Figure S13). We note also that when both IRMOF-9 and its deinterpenetrated counterpart are independently treated with a saturated

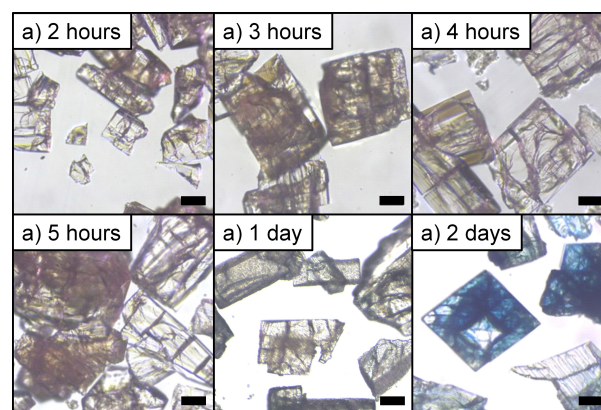


**Figure 3.** Optical microscope images of the *in situ* deinterpenetration of IRMOF-9 in the presence of Reichardt's dye. The indicated time points refer to the duration of exposure to the Et<sub>4</sub>NBr-containing conversion solution. a) 2 hours, b) 3 hours, c) 4 hours, d) 5 hours, e) 1 day, and f) 2 days. Scale bar: 50 μm.

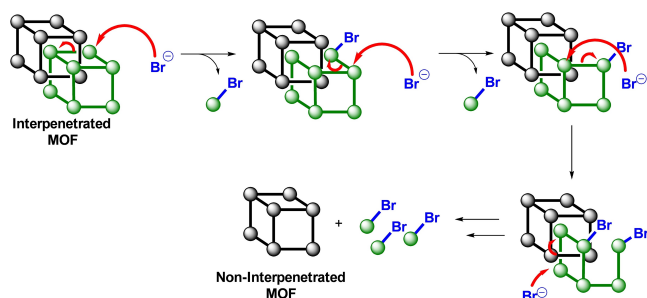


**Figure 4.** Cartoon of proposed mechanism of deinterpenetration. Note that curved arrows are a visual guide only and are not meant to fully represent the movement of electrons.

solution of ferrocene (kinetic diameter  $\sim 4$  Å) in DMF, both crystals turn yellow, demonstrating that both are porous prior to and after treatment with  $\text{Et}_4\text{NBr}$  (Figures S14). These data strongly support that IRMOF-9 was deinterpenetrated via treatment with the  $\text{Et}_4\text{NBr}$  solution.

To assess the possibility that dye inclusion could be attributed to the accumulation of mesopore and/or macropore surface defects during exposure to the  $\text{Et}_4\text{NBr}$  solution, the infiltration of cadmium selenide quantum dots (CdSe QDs) was attempted. CdSe QDs of ca. 2 nm diameter were synthesized according to a previously reported method.<sup>[20]</sup> Deinterpenetrated IRMOF-9 was then immersed in a suspension of these QDs in DCM for 12 h and subsequently washed in DCM before being analyzed via optical microscopy under UV light (Figure S15). While CdSe QDs were adsorbed to the MOF surface, penetration into the MOF interior was not observed. This observation contradicts the possibility that the successful infiltration of Reichardt's dye is attributable to meso/macropore defects from non-selective etching during the conversion process. Rather, these observations (lack of QD uptake, but successful small molecule dye uptake) are consistent with a successful deinterpenetration process that reveals larger pores of uniform diameter via the selective removal of an interpenetrating framework.

## Conclusions

The pore size distribution data, lack of low-pressure hysteresis in the gas sorption isotherm, increased BET surface area, lack of complete dissolution of the MOF in  $\text{Et}_4\text{NBr}$  solution at room temperature and presence of both BPDC and Zn in the conversion mother liquor, as well as the uptake of Reichardt's dye post conversion and subsequent exclusion of larger diameter CdSe QDs all support the preferential dissolution of a single framework. Our studies, when taken in conjunction with existing literature,<sup>[21]</sup> suggest that the mechanism of deinterpenetration involves dissolution of a single framework with minimal effect on the remaining intact framework of the MOF *within the kinetic window of the reaction* (Figure 4). We propose that this process proceeds by initial attack of the halide on one of the frameworks at the Zn-node, leading to a Zn-halide

intermediate.<sup>[11]</sup> Once this initial defect is introduced to one of the frameworks, it becomes kinetically favored to continue reacting (e.g. dissolving) over the intact framework. We speculate that initial halide attack may be assisted by defects already present in the framework due to potential partial interpenetration.<sup>[21]</sup>

In summary we have reported the deinterpenetration of IRMOF-9 by conversion via a putative dissolution mechanism. The structure of the product was confirmed via gas sorption analysis, PXRD, and size exclusion dye experiments.

## Acknowledgements

There are no conflicts to declare. This research was funded by NSF Grant DMRRUI: 1807462 (J.L.S., C.J.T., D.T.G.), the Donors of the American Chemical Society Petroleum Research Fund award #59835-DNI10 (A.B.C., J.I.F.), and the U.S. Department of Energy B.E.S. Grant No. DE-SC0004888 (C. A. C.).

## Conflict of Interests

The authors declare no conflict of interest.

## Data Availability Statement

The data that support the findings of this study are available in the supplementary material of this article.

**Keywords:** adsorption • crystal engineering • crystal growth • dyes/pigments • interpenetration • IRMOF-9 • IRMOF-10 • metal-organic frameworks • microporous materials

- [1] a) B. F. Hoskins, R. Robson, *J. Am. Chem. Soc.* **1989**, *111*, 5962–5964; b) B. F. Hoskins, R. Robson, *J. Am. Chem. Soc.* **1990**, *112*, 1546–1554; c) S. Seth, A. J. Matzger, *Cryst. Growth Des.* **2017**, *17*, 4043–4048.
- [2] a) H. Wang, J. Li, *Acc. Chem. Res.* **2019**, *52*, 1968–1978; b) Y. Wang, D. Zhao, *Cryst. Growth Des.* **2017**, *17*, 2291–2308; c) B. Li, H.-M. Wen, W. Zhou, B. Chen, *J. Phys. Chem. Lett.* **2014**, *5*, 3468–3479.
- [3] a) C.-H. Wang, W.-Y. Gao, D. C. Powers, *J. Am. Chem. Soc.* **2019**, *141*, 19203–19207; b) A. H. Chughtai, N. Ahmad, H. A. Younus, A. Laypkov, F. Verpoort, *Chem. Soc. Rev.* **2015**, *44*, 6804–6849; c) M. Viciano-Chumillas, M. Mon, J. Ferrando-Soria, A. Corma, A. Leyva-Pérez, D. Armentano, E. Pardo, *Acc. Chem. Res.* **2020**, *53*, 520–531.
- [4] a) Y. Wang, J. Yan, N. Wen, H. Xiong, S. Cai, Q. He, Y. Hu, D. Peng, Z. Liu, Y. Liu, *Biomaterials* **2020**, *230*, 119619; b) I. Abánades Lázaro, R. S. Forgan, *Coord. Chem. Rev.* **2019**, *380*, 230–259; c) L. Wang, M. Zheng, Z. Xie, *J. Mater. Chem. B* **2018**, *6*, 707–717.
- [5] a) S. Rojas, P. Horcajada, *Chem. Rev.* **2020**, *120*, 8378–8415; b) S. Kuyuldar, D. T. Genna, C. Burda, *J. Mater. Chem. A* **2019**, *7*, 21545–21576; c) X. Li, B. Wang, Y. Cao, S. Zhao, H. Wang, X. Feng, J. Zhou, X. Ma, *ACS Sustainable Chem. Eng.* **2019**, *7*, 4548–4563; d) M. Ding, X. Cai, H.-L. Jiang, *Chem. Sci.* **2019**, *10*, 10209–10230.
- [6] M. Eddaoudi, J. Kim, N. Rosi, D. Vodak, J. Wachter, M. O'Keeffe, O. M. Yaghi, *Science* **2002**, *295*, 469–472.
- [7] B. F. Abrahams, B. F. Hoskins, D. M. Michail, R. Robson, *Nature* **1994**, *369*, 727–729.
- [8] a) H.-L. Jiang, T. A. Makal, H.-C. Zhou, *Coord. Chem. Rev.* **2013**, *257*, 2232–2249; b) Y.-N. Gong, D.-C. Zhong, T.-B. Lu, *CrystEngComm* **2016**, *18*, 2596–2606; c) Q.-G. Zhai, X. Bu, X. Zhao, D.-S. Li, P. Feng, *Acc. Chem. Res.* **2017**, *50*, 407–417.

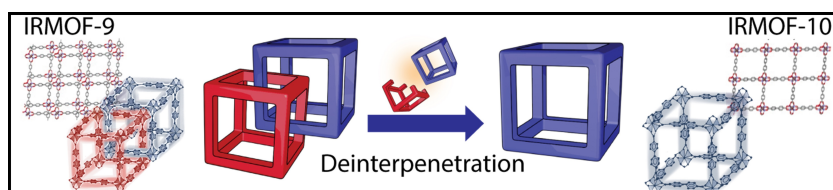
- [9] T. A. Makal, A. A. Yakovenko, H.-C. Zhou, *J. Phys. Chem. Lett.* **2011**, *2*, 1682–1689.
- [10] a) O. K. Farha, K. L. Mulfort, A. M. Thorsness, J. T. Hupp, *J. Am. Chem. Soc.* **2008**, *130*, 8598–8599; b) J. Zhang, L. Wojtas, R. W. Larsen, M. Eddaoudi, M. J. Zaworotko, *J. Am. Chem. Soc.* **2009**, *131*, 17040–17041.
- [11] M. K. Bellas, J. J. Mihaly, M. Zeller, D. T. Genna, *Inorg. Chem.* **2017**, *56*, 950–955.
- [12] a) J. L. C. Rowsell, O. M. Yaghi, *J. Am. Chem. Soc.* **2006**, *128*, 1304–1315; b) A. Khansari, M. R. Bryant, D. R. Jenkinson, G. B. Jameson, O. T. Qazvini, L. Liu, A. D. Burrows, S. G. Telfer, C. Richardson, *CrystEngComm* **2019**, *21*, 7498–7506; c) H. Khajavi, J. Gascon, J. M. Schins, L. D. A. Siebbeles, F. Kapteijn, *J. Phys. Chem. C* **2011**, *115*, 12487–12493; d) C. Wang, D. Liu, Z. Xie, W. Lin, *Inorg. Chem.* **2014**, *53*, 1331–1338; e) K. B. Sezginel, P. A. Asinger, H. Babaei, C. E. Wilmer, *Chem. Mater.* **2018**, *30*, 2281–2286; f) S. Canossa, L. Fornasari, N. Demitri, M. Mattarozzi, D. Choquesillo-Lazarte, P. Pelagatti, A. Bacchi, *CrystEngComm* **2019**, *21*, 827–834.
- [13] R. Babarao, C. J. Coghlan, D. Rankine, W. M. Bloch, G. K. Gransbury, H. Sato, S. Kitagawa, C. Sumby, M. R. Hill, C. J. Doonan, *Chem. Commun.* **2014**, *50*, 3238–3241.
- [14] S. Canossa, P. Pelagatti, A. Bacchi, *Isr. J. Chem.* **2018**, *58*, 1131–1137.
- [15] a) S. Bureekaew, H. Sato, R. Matsuda, Y. Kubota, R. Hirose, J. Kim, K. Kato, M. Takata, S. Kitagawa, *Angew. Chem. Int. Ed.* **2010**, *49*, 7660–7664; b) M. Lange, M. Kobalz, J. Bergmann, D. Lässig, J. Lincke, J. Möllmer, A. Möller, J. Hofmann, H. Krautscheid, R. Staudt, R. Gläser, *J. Mater. Chem. A* **2014**, *2*, 8075–8085.
- [16] J. I. Feldblyum, A. G. Wong-Foy, A. J. Matzger, *Chem. Commun.* **2012**, *48*, 9828–9830.
- [17] K. Banlusan, E. Antillon, A. Strachan, *J. Phys. Chem. C* **2015**, *119*, 25845–25852.
- [18] B. Liu, A. G. Wong-Foy, A. J. Matzger, *Chem. Commun.* **2013**, *49*, 1419–1421.
- [19] L. Sarkisov, A. Harrison, *Mol. Simul.* **2011**, *37*, 1248–1257.
- [20] M. L. Landry, T. E. Morrell, T. K. Karagounis, C.-H. Hsia, C.-Y. Wang, *J. Chem. Educ.* **2014**, *91*, 274–279.
- [21] a) S. Yang, X. Lin, W. Lewis, M. Suyetin, E. Bichoutskaia, J. E. Parker, C. C. Tang, D. R. Allan, P. J. Rizkallah, P. Hubberstey, N. R. Champness, K. Mark Thomas, A. J. Blake, M. Schröder, *Nat. Mater.* **2012**, *11*, 710–716; b) G. Verma, S. Kumar, T. Pham, Z. Niu, L. Wojtas, J. A. Perman, Y.-S. Chen, S. Ma, *Cryst. Growth Des.* **2017**, *17*, 2711–2717; c) D. O’Nolan, D. G. Madden, A. Kumar, K.-J. Chen, T. Pham, K. A. Forrest, E. Patyk-Kazmierczak, Q.-Y. Yang, C. A. Murray, C. C. Tang, B. Space, M. J. Zaworotko, *Chem. Commun.* **2018**, *54*, 3488–3491; d) A. Ferguson, L. Liu, S. J. Tapperwijn, D. Perl, F.-X. Coudert, S. Van Cleuvenbergen, T. Verbiest, M. A. van der Veen, S. G. Telfer, *Nat. Chem.* **2016**, *8*, 250–257; e) D. Perl, S. J. Lee, A. Ferguson, G. B. Jameson, S. G. Telfer, *Nat. Chem.* **2023**, *21*, 1358–1364.

---

Manuscript received: September 1, 2023

Accepted manuscript online: September 15, 2023

Version of record online: October 26, 2023



**A new synthesis of deinterpenetrated IRMOF-9 (IRMOF-10)** is reported using a bromide-mediated deinterpenetration of IRMOF-9 via dissolution of the second interpenetrat-

ing network. A combination of gas sorption, X-ray diffraction, and dye exclusion tests corroborate the synthesis of a deinterpenetrated IRMOF-9 product.

A. B. Crom, J. L. Strozier, C. J. Tatebe,  
C. A. Carey, Prof. J. I. Feldblyum\*,  
Prof. D. T. Genna\*

1 – 6

**Deinterpenetration of IRMOF-9**

